Reductions in California's urban fossil fuel CO_2 emissions during the COVID-19 pandemic

C. C. Yañez[1]*, F. M. Hopkins[2], X. Xu[1], J. F. Tavares[1], A. Welch[1], and C. I. Czimczik[1]*

[1]Department of Earth System Science, University of California Irvine, CA, USA 92697-3100

[2]Department of Environmental Sciences, University of California Riverside, CA, USA 92521

*Corresponding authors: Cindy Yañez (ccyanez@uci.edu), Claudia Czimczik (czimczik@uci.edu)

Key Points

- With COVID-19 restrictions, carbon dioxide levels on Los Angeles freeways were reduced by 119 ppm (or 60%) in July 2020 relative to 2019
- Plant radiocarbon analysis captured a 5 ppm reduction in Los Angeles' fossil fuel carbon dioxide levels during the Stay-At-Home order
- Mobile and plant-based measurements of fossil fuel carbon dioxide can help quantify decarbonization progress in cities

Abstract

Fossil fuel CO_2 emissions ($ffCO_2$) constitute the majority of greenhouse gas emissions and are the main determinant of global climate change. The COVID-19 pandemic caused wide-scale disruption to human activity and provided an opportunity to evaluate our capability to detect $ffCO_2$ emission reductions. Quantifying changes in $ffCO_2$ levels is especially challenging in cities, where climate mitigation policies are being implemented but local emissions lead to spatially and temporally complex atmospheric mixing ratios. Here, we assess $ffCO_2$ emission patterns associated with pandemic-induced changes to human activity using direct observations of on-road CO_2 mole fractions in the Los Angeles (LA) urban area and analyses of the radiocarbon (^{14}C) content of annual grasses collected by community scientists throughout California, USA. With COVID-19 mobility restrictions in place in 2020, we observed a significant reduction in $ffCO_2$ levels across California, especially in urban centers. In Los Angeles, on-road CO_2 enhancements were 60 ± 16% lower than the corresponding period of 2019 and rebounded to pre-pandemic levels by 2021. Plant ^{14}C analysis indicated $ffCO_2$ reductions of 5 ± 10 ppm in 2020 relative to pre-pandemic observations in LA. However, $ffCO_2$ emission trajectories varied substantially by region and sector as COVID-related restrictions were relaxed. Further development of these techniques could aid efforts to monitor decarbonization in cities, especially in developing countries without established CO_2 monitoring infrastructure.

Plain language summary

Cities emit large amounts of greenhouse gases, especially fossil fuel-derived carbon dioxide ($ffCO_2$), and thus contribute to climate change. Reducing $ffCO_2$ emissions is challenging because it is difficult to quantify the many and variable $ffCO_2$ sources of individual neighborhoods and cities. Here, we measured $ffCO_2$ reductions during the COVID-19 pandemic, demonstrating that two measurement approaches are sensitive enough to detect changes in $ffCO_2$ at fine spatial scales. We measured CO_2 levels on Los Angeles freeways using a mobile laboratory and analyzed the radiocarbon content in plant species collected by community scientists across the state of California. Both analyses indicate substantial reductions in $ffCO_2$ emissions in 2020 during California's pandemic-related shift to remote work and varying degrees of emission rebounds by 2021. We found that measurements of radiocarbon in plants is particularly sensitive to local-scale changes in human activity. Our results demonstrate that measuring the radiocarbon content of plants can serve as a useful approach to quantify local changes in cities' $ffCO_2$ patterns and monitor decarbonization as climate agreements take effect. Further development and implementation of these methods could significantly improve our shared capacity to address climate change, particularly in cities in developing countries which often lack CO_2 monitoring infrastructure.

1 Introduction

Carbon dioxide (CO_2) emissions associated with fossil fuel consumption ($ffCO_2$) are the dominant cause of climate change (IPCC, 2022). Hence, there is an urgent need to quantify $ffCO_2$ emissions to support the success of climate change mitigation efforts. Urban areas account for 30-84% of global $ffCO_2$ emissions (Seto et al., 2014), despite encompassing less than 1% of the Earth's land area (Zhou et al., 2015). While being disproportional contributors to climate change, cities are also at the forefront of climate change mitigation actions (Rosenzweig et al., 2010), making them a top priority for quantifying and monitoring $ffCO_2$ emission reduction efforts.

Satellite-borne instruments can detect CO_2 enhancements (i.e., 6 ppm above background) over large cities (Kiel et al., 2021; Schwandner et al., 2017), and urban tower networks continuously measure CO_2 levels in a small selection of cities in more economically developed countries. However, these atmospheric observation systems are limited in their ability to detect trends in $ffCO_2$ at the neighborhood scale (~1 km^2) that is needed to inform local policy makers on the outcome of mitigation actions (Duren & Miller, 2012).

The abrupt halt of economic activity at the beginning of the coronavirus disease pandemic (COVID-19), with strictest regulations in place in the U.S. from March to May of 2020, provided an unplanned experiment on the sensitivity of atmospheric greenhouse gas (GHG) observations to changes in human behavior. Restrictions intended to prevent the spread of the virus caused a wide scale disruption of human activities and consequently the largest reduction in global $ffCO_2$ emissions than has ever been observed, inducing rapid emission reductions larger than any historical human crisis or climate agreement (Le Quéré et al., 2021). These emission reductions provide insight on potential climate mitigation strategies, such as decreasing transportation emissions through increased flexibility in remote work. Several studies quantified emission reductions during the pandemic using activity-based models ("bottom up" estimates) that scale sector-based activity and consumption data with CO_2 emission coefficients. One study calculated a 17% (11 to 25%) reduction in daily global $ffCO_2$ emissions in April 2020 relative to 2019, based on a compilation of activity data and information on the intensity of mandated lockdowns (Le Quéré et al., 2020). Hourly to daily activity data indicated an overall global $ffCO_2$ decline of 8% in the first half of 2020 relative to 2019 (Liu et al., 2020).

Pandemic related emission reductions have also been assessed using atmospheric observations ("top-down" estimates). For instance, several cities have established *in situ* tower observation networks that continuously measure the total CO_2 mixing ratio. One such study reported a 30% reduction in the San Francisco Bay Area's CO_2 levels during the first six weeks of California's statewide Stay-At-Home Order (March 22 to May 4, 2020) relative to the six weeks before the order (Turner et al., 2020a). Similar reductions were reported for the Los Angeles (34 ± 6%) and Washington DC/Baltimore metropolitan areas (33 ± 11%) in April 2020 relative to the previous two years (Yadav et al., 2021). Alternative ground-based atmospheric measurements were also used to assess $ffCO_2$ emission reductions during the pandemic. Strong reductions in CO_2 fluxes (-5 to -87%) were observed during lockdown periods relative to the same times in previous years in 11 European cities using eddy-covariance measurements of CO_2 exchange (Nicolini et al., 2022). Atmospheric oxygen measurements were applied as novel tracers for $ffCO_2$ emissions in the United Kingdom and detected a 23% (14 to 32%) $ffCO_2$ reduction in 2020 annual emissions relative to a modeled scenario without the COVID-19 pandemic (Pickers et al., 2022).

Pandemic-related emission reductions were also observed in some remotely sensed data. One study combined bottom-up estimates and observations of nitrogen oxides (NO_x, pollutants that are co-emitted with CO_2 during fossil fuel combustion) from the Tropospheric Monitoring Instrument (TROPOMI) to calculate a 12% decline in China's CO_2 emissions in the first four months of 2020 relative to 2019 (Zheng et al., 2020). However, studies analyzing data from CO_2-observing satellites (such as OCO-2 and GOSAT) could not conclusively detect pandemic-related emission reductions because of sparse data retrievals, low resolution, and weak signals (Buchwitz et al., 2021; Chevallier et al., 2020).

Quantifying $ffCO_2$ emission reductions (i.e., isolating fossil fuel contributions from the total CO_2 signal) remains a key challenge for climate change mitigation efforts, especially at localized spatial scales. This is because $ffCO_2$ emissions are superimposed on large and poorly constrained fluxes from land ecosystems (e.g., photosynthesis and respirations of plants and soil microorganisms) that vary seasonally and interannually in response to temperature, the timing and amount of precipitation, drought, fire, plant life stage, and management (irrigation, harvest) as well as emissions from biofuel combustion and human metabolism (e.g., respiration, sewage). Recent work in the LA metropolitan area revealed that biospheric fluxes contribute a significant

proportion (up to 30%) to the excess level of CO_2 observed in the urban atmosphere (Miller et al., 2020). Thus, an effective $ffCO_2$ monitoring system requires a direct way to isolate fossil fuel sources from other entangled CO_2 fluxes, high spatial resolution, and accessibility to global cities.

One high resolution, sector-specific approach is the deployment of mobile GHG observatories that map fine scale patterns in $ffCO_2$ emissions from vehicle sources on urban roads (Bush et al., 2015). Such mobile measurements offer distinct sensitivity to traffic-related $ffCO_2$ emissions since the signal is dominated by nearby vehicle emissions and ambiguity related to transported air mixtures from other sources is reduced. During the COVID-19 pandemic, one mobile study observed dramatic reductions in on-road enhancements of CO_2 (-41 ppm or a 63% reduction) relative to a period before lockdowns in Beijing, China (Liu et al., 2021).

Radiocarbon analysis of plants is another promising approach for quantifying urban $ffCO_2$ trends at the local scale. Radiocarbon (^{14}C, a radioactive carbon isotope with a half-life of 5,730 years) is a unique tracer for $ffCO_2$ because fossil fuel-derived CO_2 is millions of years old and devoid of ^{14}C due to radioactive decay, while other sources of CO_2 have ^{14}C signatures similar to the current atmosphere (Graven et al., 2020; Turnbull et al., 2006; Levin et al., 2003). Currently, an input of 1 ppm of $ffCO_2$ into the atmosphere results in a depletion of ambient $\Delta^{14}CO_2$ by 2.4‰. Since plants assimilate CO_2 during photosynthesis, plant ^{14}C reflects the $^{14}CO_2$ signature of the surrounding atmosphere integrated over the period when the plants are photosynthetically active. Where $ffCO_2$ emissions dilute ^{14}C in the atmosphere, plants are depleted in ^{14}C (appear older in ^{14}C age). Thus, plants offer a natural and efficient network of ^{14}C observations and can be used to map fine-scale spatial patterns in $ffCO_2$ in places without established CO_2 monitoring infrastructure (Hsueh et al., 2007; Riley et al., 2008; Santos et al., 2019; Wang & Pataki, 2010).

Several studies have measured the ^{14}C of ambient air to quantify $ffCO_2$ trends in urban areas (Miller et al., 2020; Newman et al., 2016; Turnbull et al., 2011); however, plants offer time-integrated monitoring of ^{14}C that could more feasibly be used to monitor $ffCO_2$ spatial patterns in global cities than deploying air sampling stations at the same scale. Preparation for ^{14}C analysis is significantly faster for plant samples and can be done with just 4 mg of plant tissue since plants are approximately 40% C, while air samples (< 0.04% C) require expensive

canisters and larger volume samples (approximately 5 L) and longer processing times to get a large enough ^{14}C sample for AMS analysis. This means that more ^{14}C samples can be analyzed leading to higher spatial resolution urban $ffCO_2$ datasets than with air samples. During COVID-19 lockdowns in New Zealand, the ^{14}C of weekly-sampled grasses tracked changes in local $ffCO_2$ emissions that coincided with the stringency of COVID-related restrictions and detected a 75% ± 3 peak reduction in $ffCO_2$ emissions (Turnbull et al., 2022).

Here, we quantify changes in $ffCO_2$ emissions during select periods of the COVID-19 pandemic (spring and summer of 2020 and 2021) in California, USA, with a focus on the state's two largest urban areas: the LA metropolitan area and the San Francisco Bay Area (SFBA). The State of California is the world's fifth largest economy (based on the state's GDP of 3.36 trillion USD in 2021, bea.gov) and has enacted landmark climate action legislation. Statewide policies that restricted mobility likely altered $ffCO_2$ emission patterns during the pandemic, such as the Stay-At-Home order that required the closing of all "non-essential" businesses from March 19 to May 4, 2020 (Executive Order N-33-20). To examine the impacts of these policies on $ffCO_2$ emissions, we use two approaches that can isolate CO_2 derived from fossil sources, are spatially resolved, and do not require establishment of CO_2 monitoring infrastructure. First, we measured the mixing ratio of CO_2 on freeways in the LA area using a mobile GHG observatory. Second, we analyzed the ^{14}C content of annual grasses collected by community scientists across the state. Together, our data offer a unique insight into anthropogenic $ffCO_2$ emissions in California's urban regions during the COVID-19 pandemic and support the further use of plant ^{14}C analysis to evaluate decarbonization efforts in other cities.

2 Methods

2.1 On-road CO_2 measurements

We measured the on-road mixing ratios of CO_2 in the LA metropolitan area using a cavity ringdown spectrometer (G2401, Picarro) installed inside a mobile laboratory (2016 Mercedes Sprinter cargo van). The same platform has been used by previous studies to observe GHG and pollutant concentrations (Carranza et al., 2022; Thiruvenkatachari et al., 2020). Ambient air was continuously pumped into the Picarro from an inlet on the roof of the van behind the driver's seat, approximately 3 m above the road surface. We simultaneously collected

position and meteorological data using a global satellite positioning device (GPS 16X, Garmin) and a compact weather sensor (METSENS500, Campbell Scientific) that were mounted on the roof of the vehicle.

Measurements were collected on freeways during daytime hours on weekdays in July 2019, 2020, and 2021. We filtered the datasets from each year to only include locations that overlapped with the 2020 dataset, focusing the analysis on approximately 750 km of road. To minimize meteorological effects on our results, we only used data collected between 11 AM to 4 PM local time, when the planetary boundary layer is well-developed and surface layer air is well-mixed (Ware et al., 2016). These times exclude typical rush hour traffic periods and make our analysis conservative since rush hour emissions were likely the most strongly reduced in 2020 as commuters switched to working from home. We also filtered out data from days that were overcast and otherwise experienced similar weather conditions during all three surveys. Different filtering strategies would be required for cities that experience different meteorology than LA.

We calibrated the analyzer before and after each survey using gas cylinders with CO_2 mixing ratios that have been corrected against the NOAA WMO-CO2-X2007 scale. For each calibration, the analyzer inlet was directed to sample air from compressed gas cylinders with known mixing ratios of CO_2 for three minutes. We used two standard tanks that spanned the range of CO_2 mixing ratios we observed on the road (Table S1). We then applied a two-point correction to the data based on the linear relationship between the known and measured values. The measurements are precise to <1 ppm for all surveys based on the standard deviation of the calibration runs. The calibrated data was aggregated into 5-second intervals and gridded into 100-m road segments to synchronize trace gas, weather, and position measurements.

Urban CO_2 enhancements (CO_{2xs}) were calculated by subtracting a background that represents the CO_2 mole fraction of air coming into the LA area before it is enhanced by local emissions. For urban studies, background characterization generally depends on latitude, seasonal wind patterns, and topography. Previous studies in other cities have used CO_2 measurements from upwind rural areas or a high elevation site to represent the background (Turnbull et al., 2019; Mitchell et al., 2018). Since westerlies prevail in LA in July, a suitable background can be represented by the inflowing marine air that originates in the Pacific Ocean (Newman et al., 2016; Verhulst et al., 2017). Thus, we characterized the CO_2 background using flask sample data from NOAA's Global Monitoring Division's site at Cape Kumukahi, Hawaii

(19.54°N, 154.82°W, 15 m elevation). The NOAA GMD data is publicly available at https://gml.noaa.gov/ (Dlugokencky et al., 2021), and hosts a network of over 50 sites that monitor trace gas concentrations around the world. Previous work has found that Cape Kumukahi's CO_2 levels are similar to the local LA background for summer months (Hopkins et al., 2016). Based on the July average of all flask measurements at Cape Kumukahi, we estimate the CO_2 background was 411.0 ± 2.0 ppm in 2019, 412.9 ± 1.2 ppm in 2020, and 416.7 ± 1.7 ppm in 2021. On July 31, 2020, we measured similar CO_2 mixing ratios (413 ± 1.4 ppm) in the in-flowing marine air at Dockweiler Beach (33.94°N, -118.44°E), which supports the application of Cape Kumukahi as an adequate LA background.

We assume that the observed CO_2 enhancements are solely derived from on-road emissions. It is possible that some of these enhancements are influenced by biosphere fluxes and wildfire emissions. However, we expect that these contributions are relatively small and do not affect the results.

2.2 Radiocarbon analysis of plants

We measured the ^{14}C content of invasive annual grasses to map $ffCO_2$ trends across the state of California. The typical growing season of these species lasts from March to May, which coincided with California's statewide Stay-At-Home Order (March 19 to May 4, 2020) and made them useful bio-monitors of fossil fuel emission-reductions during the period of strictest COVID-19 measures in this area.

Because plant ^{14}C reflects the CO_2 assimilated from the atmosphere during photosynthesis, differences in ^{14}C depletion between plant samples are driven by local differences in ambient $^{14}CO_2$ composition and particularly the amount of fossil fuel influence. Studies around the world have mapped $ffCO_2$ patterns using a variety of plant species appropriate for their study area including tree rings in LA (e.g., Djuricin et al., 2012), evergreen tree leaves in Italy (Alessio et al., 2002), corn leaves in the United States (Hsueh et al., 2005) and Beijing, China (Xi et al., 2011), annual grasses in California (Riley et al., 2008; Wang & Pataki, 2010), ipê leaves in Rio de Janeiro (Santos et al., 2019), turfgrasses in New Zealand (Turnbull et al., 2022), and wheat crops in India (Sharma et al., 2022). Thus, cities can apply this technique to quantify $ffCO_2$ patterns by sampling a commonly found plant species that is photosynthetically active during the time integration period of interest. Unlike stable isotope signatures, plant ^{14}C

content does not vary based on photosynthetic pathway, water use efficiency or other growth factors. Such factors are corrected for since the measured plant $^{14}C/^{12}C$ ratios are normalized to a $\delta^{13}C$ value of -25‰. Other than fossil fuel influence, the biggest drivers of ^{14}C differences between plant species would be from the usage of stored carbon in perennial plants (Vargas et al., 2009) and from local topographic conditions (i.e., photosynthetic fixation of soil-respired CO_2 in depressions).

We recruited community scientists to collect plant samples from their neighborhoods. We distributed a packet that contained scientific background information, sampling/mailing instructions, and photos to aid with plant identification. We also held informational webinars, gave presentations at community college classrooms, and uploaded videos online demonstrating how to collect and mail the samples. Nearly 400 plant samples were submitted for the study. Most samples were collected on residential properties or along roadsides in public areas. The plant samples were mailed in paper envelopes along with the species, latitude, longitude, and date of collection. Collection dates for the samples ranged from late spring through the summer. Most plants were *Bromus tectorum* L. (cheatgrass), *Bromus diandrus* ROTH. (ripgut brome), *Avena fatua* L. (wild oat), or *Avena barbata* POTT EX LINK (slender oat). We inventoried all samples and information, confirmed their species (if identifiable), and recorded whether they were green or senesced. We also photographed all samples, focusing on their identifying features. These species represent a lower limit on annual $ffCO_2$ values since their growth period follows winter rain and wind events that cleanse pollution from the atmosphere.

We analyzed the ^{14}C content of 188 samples from the 2020 growing season and 82 samples from the 2021 growing season. We excluded plants that were not annual species, did not contain flowers, and any that showed signs of decay (rot, mold). We prioritized analysis of samples that were expected to have high $ffCO_2$ signals (urban areas) and were collected at similar locations in both years. To prepare the samples for ^{14}C analysis, we weighed out approximately 4 mg of plant tissue, focusing on flowers to target carbon fixed from the atmosphere during March to May. Samples were then sealed into pre-combusted quartz tubes with cuprous oxide, evacuated and combusted at 900°C for 3 h. The resulting CO_2 was purified cryogenically on a vacuum line, quantified manometrically, and converted to graphite using a sealed-tube zinc reduction method (Xu et al., 2007). The graphite was analyzed for ^{14}C at the W. M. Keck Carbon Cycle Accelerator Mass Spectrometer facility (NEC 0.5MV 1.5SDH-2 AMS) at

the University of California, Irvine alongside processing standards and blanks. The measurement uncertainty ranged from 1.4 to 2.1‰. We use the $\Delta^{14}C$ notation (‰) for presentation of results [Eq. 1],

$$\Delta^{14}C = 1000 \cdot (FM \cdot \exp\left(\frac{1950 - y}{8267}\right) - 1) \quad \textit{Eq. 1}$$

where y is the year of sampling, FM is the fraction modern calculated as the $^{14}C/^{12}C$ ratio of the sample divided by 95% of the $^{14}C/^{12}C$ ratio of the oxalic acid (OX) I standard measured in 1950, 8267 years is the mean lifetime of ^{14}C, and 1950 is the reference year for "modern". Mass-dependent isotopic fractionation of the sample is accounted for in the fraction modern term (Trumbore et al., 2016). This ^{14}C notation includes a correction for the decay of the OX I standard since 1950, giving the absolute ^{14}C content of our samples during the year they were collected.

We used a mass balance approach (Santos et al., 2019; Turnbull et al., 2011) to quantify the fossil fuel contribution to the local CO_2 signal (C_{ff}) at each sample location. In the following equations, C_i terms denote CO_2 mixing ratios (units of ppm) from each contributing source and Δ_i terms denote the corresponding ^{14}C signature for each source in units of per mil (‰).

$$C_{obs} \cong C_{bg} + C_{ff} \quad \textit{Eq. 2}$$

$$C_{obs}\,\Delta_{obs} \cong C_{bg}\Delta_{bg} + C_{ff}\Delta_{ff} \quad \textit{Eq. 3}$$

$$C_{ff} \cong C_{bg}\,\frac{(\Delta_{bg} - \Delta_{obs})}{(\Delta_{obs} - \Delta_{ff})} \quad \textit{Eq. 4}$$

Here, we assume the observed mixing ratio of CO_2 (units of ppm) at a location is the sum of two contributions: the CO_2 background (C_{bg}) and a fossil fuel contribution (C_{ff}) [Eq. 2]. The isoproduct for each CO_2 source must also be conserved [Eq. 3]. Combining Equations 2 and 3, we can calculate C_{ff} for each sample [Eq. 4]. All other values are known: Δ_{obs} is the measured ^{14}C content of the plant sample. For C_{bg} we use the average CO_2 mixing ratio measured at Cape Kumukahi (Dlugokencky et al., 2021) between March and May. C_{bg} was 416.7 ± 1.1 ppm for the 2020 and 419.4 ± 0.8 ppm for the 2021 growing season, respectively. The $\Delta^{14}C$ of background air (Δ_{bg}) is characterized by monthly-integrated air samples collected in a remote location Pt. Barrow, Alaska (X. Xu, Pers. Comm., 2021) and was -2.8 ± 1.3‰ for the 2020 and -6.2 ± 1.7‰ for the 2021 growing season, respectively. Δ_{ff} is -1000‰, the known fossil fuel ^{14}C signature.

Based on the average standard deviation of replicate plant samples and error propagation of the measurement uncertainty, the uncertainty in a C_{ff} estimate is 1 ppm. Our equations assume biogenic ^{14}C inputs (such as from fires or heterotrophic respiration) are small enough to be neglected in the mass balance budget. Previous work has shown that this effect is constant and relatively small (Newman et al., 2016). The plant growing season (March to May) is outside of California's wildfire season, so we do not expect wildfire emissions to affect the plant ^{14}C signatures. We also assume that the samples were not affected by ^{14}C emissions from nuclear power plants since there is only one such facility that is active in California (the Diablo Canyon Power Plant in San Luis Obispo County). The nearest plant sample was approximately 17 km northeast of the facility, which is not in the path of the area's dominant wind direction and is likely too far to intercept the emissions.

We expect that meteorology had minimal impact on our ^{14}C analysis since the plant samples experienced similar meteorological conditions across both study years, and because our plants only assimilate CO_2 during daytime hours. Thus, sampling excludes periods of strong atmospheric stability such as nighttime and early mornings that have increased CO_2 levels that are not driven by changes in $ffCO_2$ emissions (Verhulst et al., 2017; Newman et al., 2016; Djuricin et al., 2010).

3 Results and Discussion

3.1 Reduced CO_2 enhancements on Los Angeles freeways

We observed substantial reductions in on-road CO_2 enhancements (CO_{2xs}) in the LA metropolitan area during the pandemic (Fig. 1). The mean CO_{2xs} value (± SD) on LA freeways was 119 ± 50 ppm lower in July 2020 compared to July 2019 (Table 1), a -60 ± 16% change with CO_{2xs} reductions observed universally across all sampled freeways. By July 2021, COVID-related changes in behavior were reduced and CO_{2xs} rebounded by 153 ± 40 ppm compared to 2020 (Table 1). This equates to a 17 ± 29% increase in CO_{2xs} levels in July 2021 relative to July 2019. The 2021 CO_{2xs} increases were not uniformly distributed. Many freeways still had CO_{2xs} values that were lower relative to 2019, although not nearly as low as in 2020. Heavily trafficked areas had CO_{2xs} levels as much as 40% higher than 2019 (Fig. S1). Furthermore, CO_{2xs} values were less variable in 2020 (interquartile range of 33 ppm) and 2021 (interquartile range of 43

ppm) compared to 2019 (58 ppm), indicating more homogeneous CO_{2xs} on roadways during the pandemic (Fig. S2).

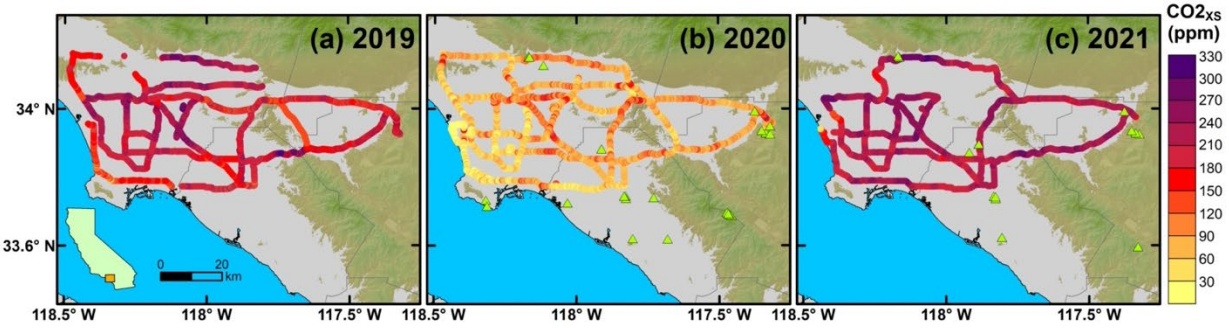

Figure 1. On-road CO_{2xs} observed near midday on Los Angeles freeways before (2019) and during the COVID-19 pandemic (2020 and 2021). Choropleth maps show CO_{2xs} observations in (a) July 2019, (b) July 2020, and (c) July 2021. Green triangles show locations of plant ^{14}C samples collected in 2020 and 2021. Basemap shows topography for elevations >300 m as hillside shading based on a Digital Elevation Model from USGS.

Changes in traffic patterns during the pandemic are likely the main cause of the changes in on-road CO_{2xs} values we observed. In addition to the number of cars on road, previous work has shown that on-road CO_2 mixing ratios are sensitive to traffic conditions such as speed, distance between cars and road grade (Maness et al., 2015). In July 2020, schools and businesses were operating in a remote or hybrid work model and many commercial facilities were closed, leading to substantial traffic reductions. Data from the California Department of Transportation's Performance Measurement System (PeMS) indicates that the vehicle miles traveled (VMT) on Southern California freeways was on average 12% lower in July 2020 compared to July 2019 (Caltrans, 2021). With fewer vehicles on the road in July 2020, there were wider distances between cars, fewer traffic jams, and fewer CO_2 emissions.

Nationwide studies conducted during the same period deduced that $ffCO_2$ emissions started recovering after reaching minima in March or April of 2020, and that by July of 2020 (our study period), the reductions had largely diminished (Harkins et al., 2021; Le Quéré et al., 2020; Liu et al., 2020). Daily ground transportation emissions in the U.S. were estimated to only be reduced by 7-8% in July 2020 compared to 2019 (Harkins et al., 2021; Liu et al., 2020). Interestingly, our LA observations indicate much larger reductions to on-road CO_2 emissions during that period (~60%). This is likely because our measurements were collected in an area

where emissions are dominated by passenger vehicles. In California and in LA, the transportation sector is the largest source of $ffCO_2$ emissions (45% of total), so changes in traffic patterns during the pandemic were more likely to have a discernable impact on this region's $ffCO_2$ budget. A 60% decrease in on-road emissions is consistent with a previous estimate that the LA area's total emissions were reduced by 30% in the spring of 2020 relative to 2018-2019 (Yadav et al., 2021). A budget balance calculation with a 30% reduction in total LA emissions in 2020 equates to a 67% reduction in on-road emissions if we assume non-vehicle $ffCO_2$ sources were held constant and the on-road sector accounted for 45% of LA's $ffCO_2$ emissions before the pandemic. However, previous studies have shown that the pandemic-related emission reductions are not completely attributable to changes in traffic (Liu et al., 2020; Yadav et al., 2021), so our ~60% reduction result is still higher than what other studies estimated. On-road CO_2 measurements are likely to detect the transportation-sector emission changes with higher sensitivity than tower- and space-based observations since signal detection is not as dependent on atmospheric transport.

Table 1

Changes in $ffCO_2$ levels during the COVID-19 pandemic in California based on on-road mobile surveys and observations of ^{14}C in plants and/or air

Region	Pre-pandemic	2020	2021	COVID-19[a]	Rebound[b]
CO_{2xs} (ppm) via on-road mobile surveys					
LA	199 ± 42[c]	80 ± 27	233 ± 29	-119 ± 50*	153 ± 40*
$ffCO_2$ (ppm) based on ^{14}C in plants and/or air					
CA	4 ± 5[d]	4 ± 4	5 ± 5	0 ± 6	1 ± 6
co-located	*n.a.*	*5 ± 5*	*5 ± 6*	*n.a.*	*0 ± 8*
LA	11 ± 9[e]	6 ± 5	9 ± 7	-5 ± 10*	3 ± 9
co-located	*n.a.*	*9 ± 9*	*11 ± 10*	*n.a.*	*2 ± 13*
Pasadena	23 ± 4[f]	3	13 ± 2	-20 ± 4*	10 ± 2*
Irvine	7 ± 4[g]	6	4 ± 1	-1 ± 4	-2 ± 1

Notes: Asterisk (*) indicates the means were significantly different based on Welch's t-test. Further details for these calculations are in Table S2. Uncertainties are standard deviations. Values that do not have uncertainties indicate a sample size of 1. For these cases, the uncertainty in the $ffCO_2$ estimate is assumed to be 1 ppm based on the differences in replicated plant samples. Values in regular font represent all the samples collected in that year, while values in italicized font represent only co-located plant samples that were collected in both 2020 and 2021 less than 150 m apart.

[a]Calculated as the difference between the 2020 (intense physical distancing measures and mobility restrictions) and pre-pandemic columns. The pre-pandemic observations are based on datasets from various years and are described in the subsequent footnotes and Table S2.

[b]Calculated as the difference between 2021 and 2020 (relaxation of physical distancing measures and mobility restrictions)

[c]July 2019 on-road mobile measurements.

[d]2005 plant ^{14}C observations (Riley et al., 2008).

[e]Based on 2005 plant ^{14}C observations (Wang & Pataki, 2010) and 2015-2016 air ^{14}C samples (Miller et al., 2020).

[f]Predicted value based on a linear extrapolation of 2006-2013 air ^{14}C samples (Newman et al., 2016) assuming the trend continued and there had been no pandemic.

[g]2019 air ^{14}C samples (Xu, pers. Comm., 2020).

While our data revealed striking reductions in CO_2 mixing ratios, it is not trivial to translate changes in on-road CO_2 mixing ratios into reductions in CO_2 emissions. One reason for this is confounding effects of changes in vehicle speeds on CO_2 emissions. There is a nonlinear relationship between vehicle speeds and emission rates, such that vehicles emit more CO_2 at very low and very high speeds (Fitzmaurice et al., 2022). In 2020, our average speed was 9 km h^{-1} faster than 2019 and 12 km h^{-1} faster than 2021, which suggests a decrease in congestion in 2020. Within the range of our average speeds (64 to 76 km/hr), there is not expected to be a substantial change in CO_2 emission rates (Fitzmaurice et al., 2022). However, these averages do not capture the non-constant speeds during periods of congestion that make vehicles less efficient and increase both CO_2 emissions (Barth and Boriboonsomsin, 2008) and roadway enhancements. Faster speeds produce more CO_2 emissions because vehicle engines are doing more work and using more fuel, but they also create more turbulence near the road that effectively mixes vehicle emissions, thereby reducing on-road CO_2 enhancements. Nonetheless, we did not find a significant relationship between our measurements of CO_{2xs} and vehicle speed (Fig. S3). We estimated how much vehicle speed would affect our measurements using a model where on-road CO_{2xs} levels scale with vehicle speed to a power of -⅓ (Baker, 1996; Maness et al., 2015). Assuming that total highway emissions (Q) are related to CO_{2xs} and vehicle speed (v) by Equation 5 where κ is a constant of proportionality based on theoretical atmosphere and traffic conditions, a 9 km/hr increase in speed as observed in 2020 only causes total emissions to increase by less than 5%. Thus, we attribute the measured CO_{2xs} reductions to the smaller number of cars on the road, not the changes in speed.

$$CO_{2xs} = \kappa Q v^{-1/3} \qquad \textit{Eq. 5}$$

Interestingly, our on-road observations did not scale proportionally with vehicle miles traveled (VMT), a metric that has been used to infer $ffCO_2$ emissions from the transportation sector (Gurney et al., 2020; Gately et al., 2015). While we observed a 60 ± 16% reduction in CO_{2xs} in July 2020 relative to July 2019, VMT in the LA area was only reduced by 12% during the same time periods (CalTrans, 2021). VMT does not adequately capture the strong CO_2 signal we observed because it does not account for the effects of driving behavior, congestion, vehicle speeds, and fleet composition on CO_2 emissions (Rao et al., 2017), all of which likely changed during 2020. While relationships between emissions and speed are incorporated in some models,

412 less work has incorporated the effects of stop-and-go driving, which is likely to produce higher
413 CO_2 emissions. Less congestion in 2020 could have reduced CO_2 emissions in ways that have
414 not been fully explored. Other studies also reported large discrepancies between $ffCO_2$ emission
415 estimates based on governmental traffic data, fuel-based models, and novel cell phone-based
416 mobility datasets (Gensheimer et al., 2021; Harkins et al., 2021; Oda et al., 2021). Future work is
417 needed to consolidate these different metrics for estimating transportation $ffCO_2$ emissions and
418 to better understand what information each of these datasets represents.

419 Assuming the measured 60% reduction in on-road CO_{2xs} translates into a 60% reduction
420 in annual interstate $ffCO_2$ emissions (7.6 Mt C yr^{-1} in 2012; Rao et al., 2017), given that
421 interstates are the primary road type included in this analysis, this equates to an avoided 4.6 Mt
422 C. The estimated total emissions for the LA area was 47.2 ± 5.2 Mt C yr^{-1} in 2015 (Gurney et al.,
423 2019). This would imply that LA's total $ffCO_2$ emissions were reduced by 10% if all the
424 pandemic-induced reductions in 2020 were solely due to changes to on-road interstate emissions
425 (neglecting $ffCO_2$ changes in other sectors, such a residential, industry, and non-interstate roads).
426 Interstate emissions constitute only 40% of LA's on-road emissions (Rao et al., 2017). If we
427 instead assume the COVID-induced traffic reductions resulted in a 60% reduction in $ffCO_2$ for
428 the entire on-road sector (including all road types), then $ffCO_2$ emissions were reduced by 11.4
429 Mt C, or 24% of LA's total $ffCO_2$ emissions.

430 **3.2 Reduced $ffCO_2$ emissions during the Stay-At-Home order**

431 ^{14}C analyses of plant species were used to map $ffCO_2$ patterns, whereby lower $\Delta^{14}C$
432 values indicate higher $ffCO_2$ inputs (Fig. 2). In 2020, the average $\Delta^{14}C$ (± SD) was -11.3 ± 8.6‰
433 (n=188) statewide, and -15.9 ± 12.5‰ (n=53) in the LA area, -10.2 ± 5.5‰ (n=91) in the SFBA,
434 and -10.3 ± 5.6‰ (n=12) in the San Joaquin Valley. This equates [*Eq. 4*] to average fossil fuel
435 contributions of 4 ± 5 ppm statewide, and 6 ± 5 ppm in the LA area, 3 ± 2 ppm in the SFBA, and
436 3 ± 2 ppm in the San Joaquin Valley. The cleanest samples were found in California's northern
437 coast ($\Delta^{14}C$ of -5.3 ± 3.7‰, n = 5). Generally, $\Delta^{14}C$ of plants collected in urban areas were more
438 depleted and more variable than in non-urbanized regions, indicating higher and locally variable
439 emissions of $ffCO_2$ (Fig. 2). Sample collection was biased toward urban areas, with 77% of
440 samples collected either in the LA area or SFBA, leading to higher uncertainty in predictions in
441 other regions of the state (Fig. S4). However, we expect rural and remote areas such as northern

442 California and the Sierra Nevada Mountains to have similar ^{14}C values as the background and
443 little variability (Riley et al., 2008). Thus, while we do not have a lot of plant samples in these
444 areas, we do not expect to see substantial COVID-effects on $ffCO_2$ levels.

445

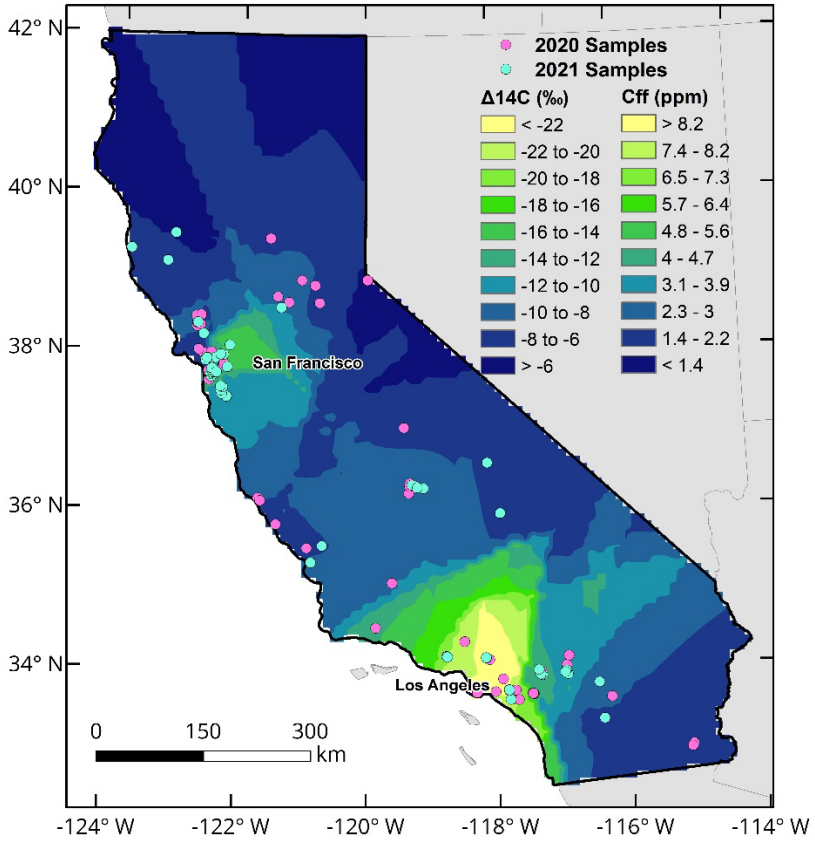

446

447 **Figure 2.** The $\Delta^{14}C$ (‰) of annual grass samples collected in California, USA and the
448 corresponding C_{ff} values in 2020. Blue points indicate locations where plants were collected in
449 both 2020 and 2021, while pink points indicate 2020-only locations. Background colors were
450 mapped using an ordinary kriging interpolation of 2020 plant $\Delta^{14}C$ values using the Spatial
451 Analyst toolbox in ESRI's ArcMap software. The uncertainty in the kriging prediction is
452 presented in Fig. S4.

453

454 To assess our 2020 plant ^{14}C observations in the context of long-term trends in the region,
455 we compared our data to existing records of ^{14}C in plants and/or air from Irvine, CA (a coastal
456 city south of LA) and Pt. Barrow, AK (a remote location far from $ffCO_2$ sources) (Fig. 3).

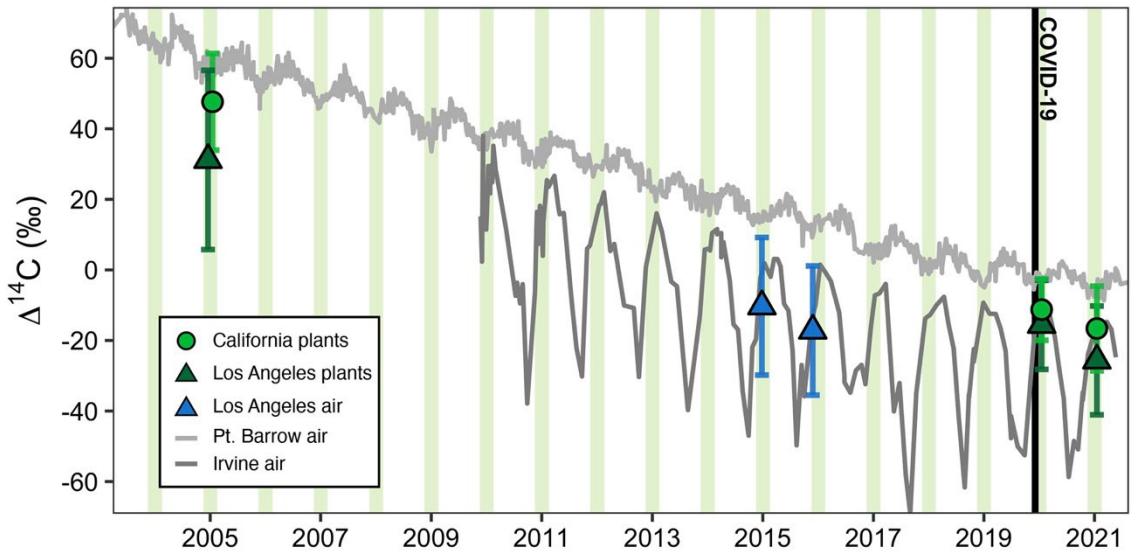

Figure 3. A record of $\Delta^{14}C$ measurements from 2003-2021. Average plant ^{14}C from various studies are shown as green points with error bars showing the standard deviation. Green circles represent statewide data (this study and Riley et al. 2008) while triangles represent only the Los Angeles metropolitan area (this study and Wang & Pataki, 2010). Air-based ^{14}C observations are shown as gray lines (X. Xu, Pers. Comm., 2021) and blue triangles (Miller et al., 2020). Shaded green bars represent the typical annual grass growing season in California (March to May).

We infer urban $ffCO_2$ emission reductions during the 2020 Stay-At-Home order relative to the ^{14}C records shown in Fig. 3 based on two metrics: variability in ^{14}C (standard deviation of mean) and the difference in ^{14}C from the hemispheric background (Pt. Barrow, Alaska). Reduced variability in ^{14}C indicates reduced $ffCO_2$ levels since emissions lead to anomalous and spatially variable ^{14}C values. The standard deviations of plant $\Delta^{14}C$ samples collected in the LA metropolitan area were 25.4‰ in 2005 (n=79, Wang & Pataki, 2010), 12.5‰ in 2020 (n=53), and 15.4‰ in 2021 (n=27). Thus, plant ^{14}C was less variable during California's 2020 Stay-At-Home order.

Furthermore, 2020 samples were more similar to the hemispheric background than in other years. Compared to Pt. Barrow, LA area ^{14}C samples were depleted by 26 ± 3‰ in 2005 (plant samples; Wang & Pataki, 2010), 25 ± 2‰ in 2015, 30 ± 4‰ in 2016 (flask samples; Miller et al., 2020), 13 ± 2‰ in 2020, and 19 ± 3‰ in 2021 (this study's plant samples; average depletion ± standard error of the mean). The mean 2020 depletion is significantly smaller than pre-pandemic years to a 95% confidence interval, indicating that $ffCO_2$ levels were reduced in

2020. Translating the ^{14}C depletion from background into fossil fuel-sourced CO_2 enhancements [*Eq. 4*], the mean C_{ff} in LA during pre-pandemic years ranged from 10-13 ppm (Table S2). However, during the pandemic the mean C_{ff} reduced to 6 ± 5 ppm (Table 1). Thus, we calculate $ffCO_2$ levels were reduced by 5 ± 10 ppm relative to pre-pandemic observations.

These samples reflect varying locations within the Los Angeles region, and hence we are assuming that both prior and current plant samples as well as previous flask samples are similarly representative of the region. To minimize the impact of these assumptions, we also estimated $ffCO_2$ emission reductions in one location, Pasadena, a city in the northeast LA basin that receives polluted air from the LA region during afternoon hours (Newman et al., 2008). Based on a linear extrapolation of the Pasadena air record (Newman et al., 2016), the mean $\Delta^{14}C$ during the 2020 growing season (March to May) would have been -55.5 ± 8.8‰ had there been no pandemic, translating to a local enhancement of 23 ± 4 ppm CO_2 above background [*Eq. 4*], but a plant sample collected in 2020 approximately 4 km away had an enhancement of only 3 ± 1 ppm CO_2 (Fig. 4). This difference indicates a reduction of 20 ± 4 ppm $ffCO_2$ in Pasadena during the 2020 Stay-At-Home order. In 2021, plants were sampled in this location again and had an average $\Delta^{14}C$ of -35.7 ± 4.5 ‰ (n=6), an enhancement of 13 ± 2 ppm CO_2. This value is closer to, but still significantly different from, the predicted 2021 mean value (-60 ± 9.4‰ or 24 ± 5 ppm CO_2 enhancement), indicating a partial but not complete rebound to the pre-pandemic emissions trend. In summary, we found that plant ^{14}C data was able to capture interannual changes in local $ffCO_2$ during the pandemic.

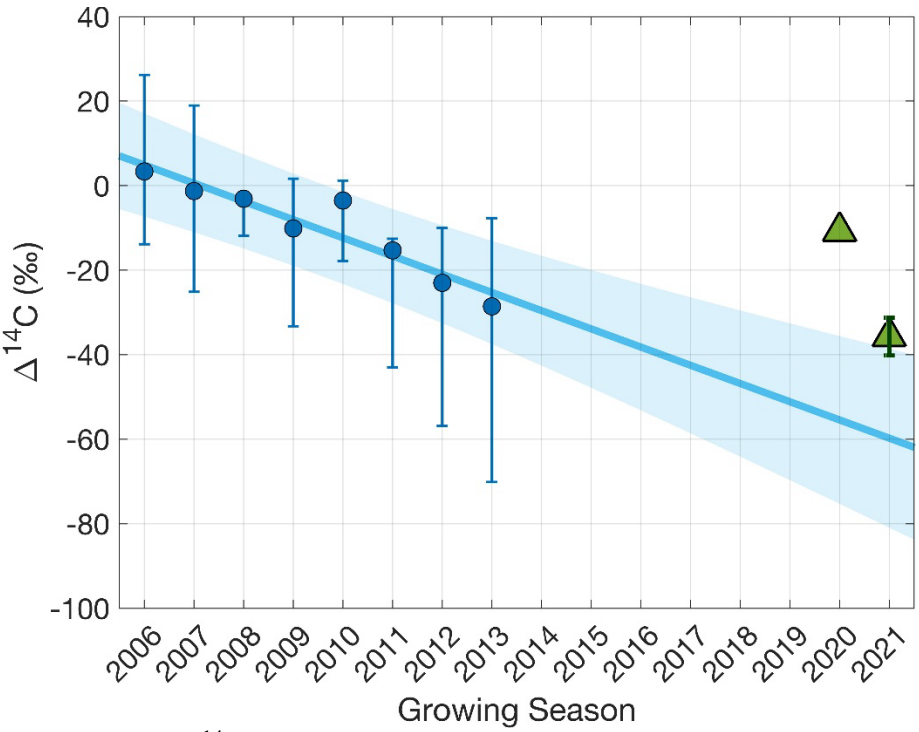

Figure 4. Growing season $\Delta^{14}C$ of ambient CO_2 in Pasadena, CA, a city within the northeast Los Angeles basin. The blue circles show the average growing season (March to May) $\Delta^{14}C$ of ambient CO_2 at Caltech [*Newman et al., 2016*], with error bars showing the minimum and maximum $\Delta^{14}C$ measurements. The line is a linear regression of these data with shading indicating the 95% confidence intervals. The green triangles show the measured $\Delta^{14}C$ of plant samples collected approximately 4 km away from the Caltech site in 2020 (n=1) and 2021 (n=6, error bars show standard deviation).

3.3 Changes in $ffCO_2$ during the rebound period (2020 to 2021)

Although the pandemic continued into the 2021 growing season, virus-restricting mandates were relaxed and California's vehicle miles traveled were 30% higher than the same period in 2020 (Caltrans, 2021). We observed large spatial variations and heterogeneity in ^{14}C during the second spring and summer of the pandemic. Based on a subset of samples collected at similar locations (< 150 m away) in both 2020 and 2021, we find that $ffCO_2$ levels did not change significantly between 2020 and 2021 at the statewide scale, with a mean change of 0 ± 8 ppm (Table 1). This average belies significant local variability in changes in $\Delta^{14}C$ between 2020 to 2021 (Fig. S5). The disparity in $ffCO_2$ emission rebounds in 2021 could be related to variations in pandemic responses as the economy recovered after the Stay-At-Home Order. We observed larger emission rebounds in LA than SFBA (Figs. 5 & S6). SFBA had more instances of $\Delta^{14}C$ values that either increased or only decreased as much as the long-term global ^{14}C trend between 2020 and 2021. The SFBA had a slower relaxation of COVID-19 prevention measures

than other regions of California. Here, and also in Orange County in the LA area, many people continued to work from home into 2021, which may explain why emission reductions generally persisted even after lockdown restrictions were lifted (blue areas in Fig. 5a,b). In LA neighborhoods, working from home was not an option for many "essential" workers, which might contribute to samples showing a stronger emission rebound in 2021 (red areas in Fig. 5b). These neighborhoods also have a greater density of freeways.

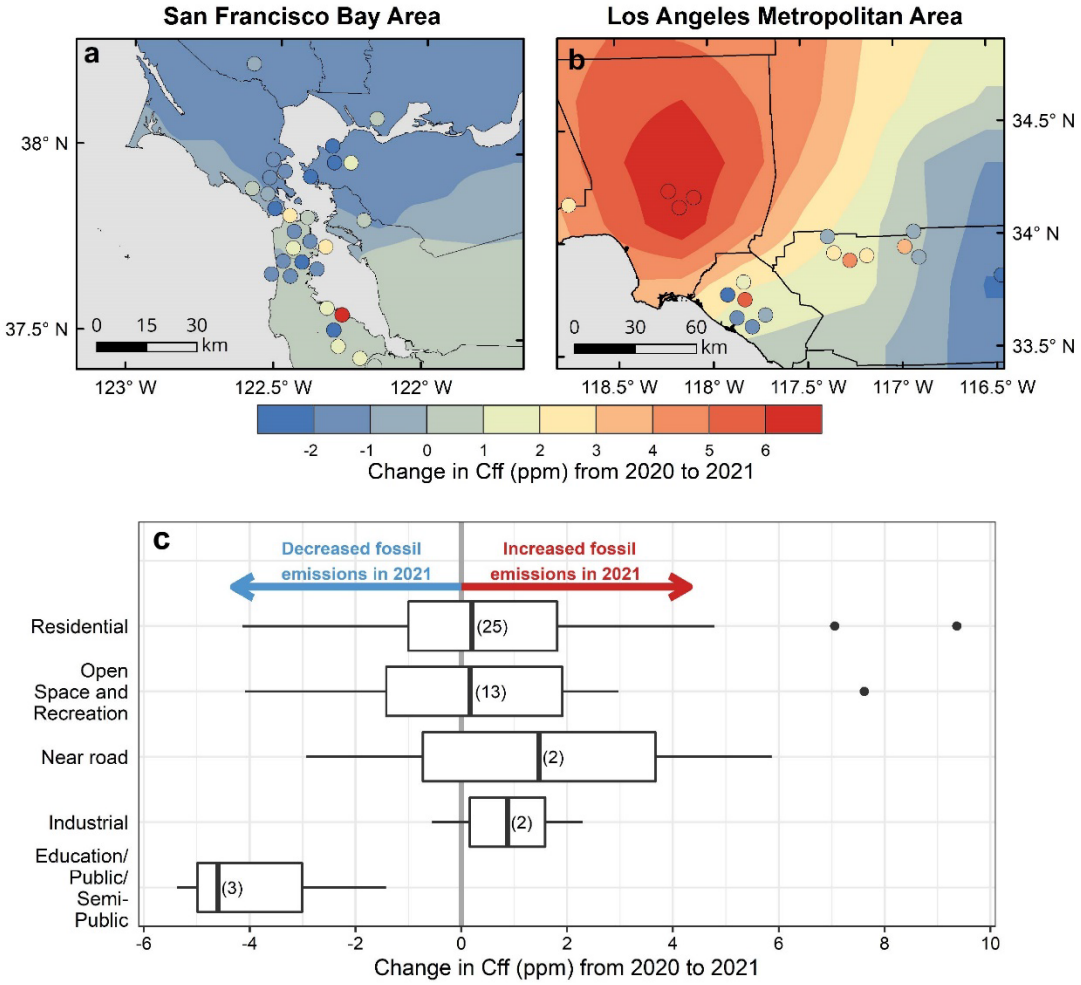

Figure 5. The difference in C_{ff} values from 2020 to 2021 between plant samples repeatedly collected in California's urban areas: (a) the San Francisco Bay Area and (b) the Los Angeles metropolitan area. Points show sample locations colored by their change in C_{ff}. Redder colors indicate $ffCO_2$ emission increases in 2021 compared to 2020. Background colors were calculated using an Ordinary Kriging interpolation of C_{ff} in ESRI's ArcMap software. C_{ff} changes by land use class are shown in (c).

We used city land use data to further investigate the $ffCO_2$ emission sectors represented by plant samples collected in the LA area and SFBA (45 sample pairs, Fig. 5c). We found that the majority of plants were collected in areas classified as residential (58% of paired samples) or open space/recreation (29%). While there is large variation in ^{14}C within each category and results indicate that heterogeneity within regions/sectors was larger than the COVID-induced changes, there is a small trend toward higher $ffCO_2$ emissions in residential, open space/recreation and industrial areas, and a trend toward lower emissions from educational and public spaces. This is consistent with a return to normal of many activities, whereas schools in California stayed closed through the 2021 growing season and many government sector employees continued work from home. These sector-averaged trends are larger when all data is used (Fig. S7) but are on the order of ±1-2 ppm, which is not much larger than the uncertainty in our C_{ff} estimates (±1 ppm).

The heterogeneity in year-to-year changes elucidates the highly localized sensitivity of plant ^{14}C and indicates that this approach is a simple, yet effective method to monitor interannual changes in the $ffCO_2$ burden at the neighborhood scale. Thus, this approach could effectively track changes in local emissions if plants are periodically collected in direct proximity (< 20 m) from $ffCO_2$ emission sources. For instance, the Great Highway, a major north-south thoroughfare on San Francisco's western edge, was closed to vehicles from April 2020 to August 2021. The road was converted into a car-free active transportation route, with access permitted only to pedestrians and bicyclists. Vehicle traffic was rerouted to 19th Avenue, a portion of CA State Route 1 less than 3 km east of the Great Highway. In 2020, plants collected along these two roads had very similar $\Delta^{14}C$ values (0.8‰ difference, which is within the measurement uncertainty). In 2021, a plant collected on the Great Highway was still statistically indistinguishable from the 2020 samples (0.7‰ difference), while a plant sample collected on 19th Avenue was significantly more depleted relative to the 2020 sample (-24.8‰ difference, equivalent to an increase of 10 ppm C_{ff}). This indicates higher $ffCO_2$ emissions on 19th Avenue where traffic increased in 2021, while $ffCO_2$ emission reductions near the Great Highway persisted while the roadway remained closed to vehicles.

All in all, we observed varying degrees of $ffCO_2$ reductions and rebound during the COVID-19 pandemic at various domains and spatiotemporal scales (Table 1). Year-to-year

differences were more evident in urban domains (i.e., LA, Pasadena) than in statewide means or in coastal samples (e.g., Irvine).

3.4 Best practices and recommendations for future plant radiocarbon studies

Future work should conduct strategic experiments to better understand the correspondence between plant ^{14}C and other $ffCO_2$ atmospheric monitoring metrics. This will improve the applicability of plant ^{14}C analysis as a tool for monitoring decarbonization in cities around the world. Plant ^{14}C analysis reflected trends in ambient $\Delta^{14}CO_2$, with plant values having reasonable correspondence with air records from Irvine, CA and Pt. Barrow, AK (Fig. 3). However, our plant ^{14}C-based results contrast with our on-road CO_{2xs} observations where we observed a return to pre-pandemic conditions by July 2021. This is because the two datasets represent different emission sources and geographic regions. While the CO_{2xs} data specifically represents the LA area's on-road sector, our plant samples are mainly representative of statewide residential, open space and recreational areas, which showed a more heterogeneous response to the lifting of COVID-related restrictions. No plant samples were collected within 500-m of the roads surveyed with the mobile observatory (Fig. 1), so the two datasets were not directly comparable. A more strategic sampling approach could reveal the relationship between these two approaches and the capacity of plants to monitor changes in transportation-sector emissions.

The spatial sensitivity ("footprint") of a plant is expected to be very localized (<100 m) but may vary for each sample depending on the local topography and air ventilation conditions. Previous work has shown that plants are predominantly influenced by emissions within 20 to 40 m (Lichtfouse et al., 2005; Turnbull et al., 2022). In contrast, atmospheric CO_2 measurements from rooftop/tower sites integrate signals over larger spatial scales (~10 km) since the inlet is higher above the ground (Kort et al., 2013). This makes tower sites well-suited for continuous monitoring of net $ffCO_2$ trends over an entire city using the CO_2 differential between a set of inflow- and outflow-representative sites. However, the localized spatial sensitivity of plants could be advantageous for studies seeking to investigate emissions at the neighborhood scale or from specific $ffCO_2$ sources (i.e. individual facilities or roads). Such analyses would require a strategic sampling design, targeting specific emission sources such as major roads (Turnbull et al., 2022). Without such targeted sampling, aggregated plant ^{14}C results in complex urban environments can be difficult to interpret since they represent highly local $ffCO_2$ emissions that

may vary based on individual and immeasurable factors (i.e., human behaviors) within a neighborhood. With appropriately targeted sample pairs, however, plant ^{14}C can effectively reveal $ffCO_2$ reduction outcomes of local decarbonization measures (e.g., the Great Highway case described in Section 3.3). Plant-based monitoring of $ffCO_2$ emissions could also potentially be an appropriate proxy for exposure to co-emitted air pollutants such as from vehicle traffic and may be able to elucidate environmental justice concerns between neighborhoods. Future investigations are needed to assess this.

It is important to constrain the timing of carbon uptake as much as possible to distinguish spatially driven changes from temporal changes. Atmospheric $^{14}CO_2$ undergoes large temporal oscillations (Fig. 5) with the amplitude and seasonality driven by the timing of ^{14}C production and descendance into the troposphere, natural and anthropogenic CO_2 fluxes, and seasonal meteorology (wind and air mixing conditions). While the timing of flask sample collection is well-known, the timing of CO_2 uptake by plants is more uncertain. However, plant samples compensate for that by integrating over daytime hours of their photosynthetic period, hence, reducing significant short-term variability observed in flask samples (e.g., Miller et al., 2020) to yield a seasonal average $ffCO_2$.

By sampling annual grasses, we have assumed that our $\Delta^{14}C$ analysis represents the growing season of these species in the region. We verified this assumption using downscaled remotely sensed observations of solar induced fluorescence (SIF, Fig. S8) (Turner et al., 2020b) from the TROPOMI instrument onboard the Sentinel-5 Precursor satellite. Using the date of maximum SIF observance to represent the timing of peak growth, we found that all senesced plants had peak growth dates from March to May. We also observed some temporal agreement between plant $\Delta^{14}C$ and ambient $\Delta^{14}CO_2$ measured in Irvine, CA (Figs. S8 & S9), indicating potential applications of plant ^{14}C at the sub-seasonal scale. However, many $\Delta^{14}C$ values did not coincide with the Irvine trend and were more strongly driven by their distance to major roads (Fig. S8c), showing that the main driver of the samples' ^{14}C content is proximity to $ffCO_2$ emissions, with seasonality a secondary driver. SIF observations can help constrain the timing of plant growth for future studies to disentangle the spatial and temporal drivers of plant ^{14}C. Future studies could also potentially use purposely grown plants to monitor $ffCO_2$ (i.e., turfgrasses, Fig. S9), and actively manage the growing period to the timing of interest, which would allow similar

analyses at smaller time scales and for other times of the year besides the annual grass growing season.

4 Conclusions

We quantified changes in fossil fuel consumption during the COVID-19 pandemic when California implemented aggressive mitigation measures, that included Stay-At-Home and work-from-home orders, travel limitations, and experienced widespread economic shutdown. On-road surveys of excess CO_2 demonstrated a drastic but temporary reduction in $ffCO_2$ emissions on LA freeways, with only about half the typical $ffCO_2$ emissions in July of 2020 and a return to pre-pandemic levels by July 2021. The analysis of ^{14}C in annual plants also revealed a measurable reduction in LA's $ffCO_2$ emissions in the spring of 2020 and 2021, indicated by a smaller offset between plant ^{14}C and ^{14}C of well-mixed northern hemispheric CO_2, and less variation in plant ^{14}C compared to previous years.

Our complementary approaches captured the heterogeneous reality of mandated and voluntary movement restrictions in California during the pandemic. Our study focused on a region rich in high quality datasets (i.e., previous ^{14}C records, a neighborhood scale bottom-up inventory, and an *in-situ* tower network) which allowed us to assess $ffCO_2$ emission reductions in the context of long-term trends. Mobile surveys can detect year-to-year differences in $ffCO_2$ trends from the on-road sector with high confidence, but further work is needed to relate on-road CO_2 enhancements to vehicle emissions and their drivers. Future research to constrain the spatial and temporal representation of periodically surveyed plants can support the tracking of decarbonization outcomes in cities and neighborhoods without investment in energy- and maintenance-demanding infrastructure. To account for the extreme variability of emissions sources in urban environments, however, plant-based $ffCO_2$ monitoring should focus on temporally-repeated sampling of active plants in well-ventilated areas in the direct vicinity of specific emission sources.

Acknowledgments

The authors wish to thank all community scientists who submitted plant samples for this study and the Amigos de Bolsa Chica for helping with recruitment. Additionally, we thank A. Ocampo, C. Gurguis, V. Carranza, A. Odwuor, and C. Limón for their assistance with mobile

surveys and W. M. Keck Carbon Cycle Accelerator Mass Spectrometer facility staff for supporting isotope analyses. We also thank A. Turner for his insight on this manuscript and for providing the downscaled solar induced fluorescence data to support the analysis. C. C. Yañez received support for this work from the National Science Foundation Graduate Research Fellowship Program (DGE-1839285). We also acknowledge helpful comments from three anonymous reviewers and editor E. Davidson.

Conflict of Interest Statement

The authors declare no conflicts of interest.

Open Research

The datasets of on-road CO_2 and plant radiocarbon are available in the Dryad public data repository and can be accessed via https://doi.org/10.7280/D1F98G (Yañez et al., 2022). The city land use datasets are administered by the Association of Bay Area Governments, the Metropolitan Transportation Commission, and the Southern California Association of Governments. These datasets are available in the public domain:

https://opendata.mtc.ca.gov/datasets (Planned Land Use 2005);

https://gisdata-scag.opendata.arcgis.com/datasets (2019 Annual Land Use Dataset (ALU v.2019.2))

References

Alessio, M., Anselmi, S., Conforto, L., Improta, S., Manes, F., & Manfra, L. (2002). Radiocarbon as a biomarker of urban pollution in leaves of evergreen species sampled in Rome and in rural areas (Lazio—Central Italy). *Atmospheric Environment*, *36*(34), 5405-5416.

Baker, C. J. (1996). Outline of a novel method for the prediction of atmospheric pollution dispersal from road vehicles. *Journal of Wind Engineering and Industrial Aerodynamics*, *65*, 395–404.

Barth, M., & Boriboonsomsin, K. (2008). Real-world carbon dioxide impacts of traffic congestion. *Transportation research record*, *2058*(1), 163-171.

Buchwitz, M., Reuter, M., Noël, S., Bramstedt, K., Schneising, O., Hilker, M., Fuentes Andrade, B., Bovensmann, H., Burrows, J. P., di Noia, A., Boesch, H., Wu, L., Landgraf, J., Aben, I., Retscher, C., O'Dell, C. W., & Crisp, D. (2021). Can a regional-scale reduction of atmospheric CO2during the COVID-19 pandemic be detected from space? A case study for East China using satellite XCO2 retrievals. *Atmospheric Measurement Techniques*, *14*(3), 2141–2166. https://doi.org/10.5194/amt-14-2141-2021

687 Bush, S. E., Hopkins, F. M., Randerson, J. T., Lai, C. T., & Ehleringer, J. R. (2015). Design and
688 application of a mobile ground-based observatory for continuous measurements of atmospheric
689 trace gas and criteria pollutant species. *Atmospheric Measurement Techniques*, *8*(8), 3481–3492.
690 https://doi.org/10.5194/amt-8-3481-2015
691 Caltrans, California Department of Transportation. (2021). Caltrans, California Department of
692 transportation. Performance Measurement System Data Source. Retrieved from
693 http://pems.dot.ca.gov/
694 Carranza, V., Biggs, B., Meyer, D., Townsend-Small, A., Thiruvenkatachari, R. R., Venkatram, A.,
695 Fischer, M. L., & Hopkins, F. M. (2022). Isotopic Signatures of Methane Emissions From Dairy
696 Farms in California's San Joaquin Valley. *Journal of Geophysical Research: Biogeosciences*,
697 *127*(1), 1–15. https://doi.org/10.1029/2021JG006675
698 Chevallier, F., Zheng, B., Broquet, G., Ciais, P., Liu, Z., Davis, S. J., Deng, Z., Wang, Y., Bréon, F. M.,
699 & O'Dell, C. W. (2020). Local Anomalies in the Column-Averaged Dry Air Mole Fractions of
700 Carbon Dioxide Across the Globe During the First Months of the Coronavirus Recession.
701 *Geophysical Research Letters*, *47*(22). https://doi.org/10.1029/2020GL090244
702 Djuricin, S., Xu, X., & Pataki, D. E. (2012). The radiocarbon composition of tree rings as a tracer of local
703 fossil fuel emissions in the Los Angeles basin: 1980–2008. *Journal of Geophysical Research:*
704 *Atmospheres*, *117*(D12).
705 Dlugokencky, E.J., J.W. Mund, A.M. Crotwell, M.J. Crotwell, and K.W. Thoning (2021), Atmospheric
706 Carbon Dioxide Dry Air Mole Fractions from the NOAA GML Carbon Cycle Cooperative
707 Global Air Sampling Network, 1968-2020, Version: 2021-07-30, https://doi.org/10.15138/wkgj-
708 f215
709 Duren, R. M., & Miller, C. E. (2012). Measuring the carbon emissions of megacities. In *Nature Climate*
710 *Change* (Vol. 2, Issue 8, pp. 560–562). Nature Publishing Group.
711 https://doi.org/10.1038/nclimate1629
712 Eldering, A., Taylor, T. E., O'Dell, C. W., & Pavlick, R. (2019). The OCO-3 mission: Measurement
713 objectives and expected performance based on 1 year of simulated data. *Atmospheric*
714 *Measurement Techniques*, *12*(4), 2341–2370. https://doi.org/10.5194/amt-12-2341-2019
715 Fitzmaurice, H. L., Turner, A. J., Kim, J., Chan, K., Delaria, E. R., Newman, C., Wooldridge, P., &
716 Cohen, R. C. (2022). Assessing vehicle fuel efficiency using a dense network of CO2
717 observations. *Atmospheric Chemistry and Physics*, *22*(6), 3891–3900.
718 https://doi.org/10.5194/acp-22-3891-2022
719 Gately, C. K., Hutyra, L. R., & Sue Wing, I. (2015). Cities, traffic, and CO2: A multidecadal assessment
720 of trends, drivers, and scaling relationships. *Proceedings of the National Academy of*
721 *Sciences*, *112*(16), 4999-5004.
722 Gensheimer, J., Turner, A. J., Shekhar, A., Wenzel, A., Keutsch, F. N., & Chen, J. (2021). What Are the
723 Different Measures of Mobility Telling Us About Surface Transportation CO2 Emissions During
724 the COVID-19 Pandemic? *Journal of Geophysical Research: Atmospheres*, *126*(11), 1–11.
725 https://doi.org/10.1029/2021JD034664
726 Graven, H., Keeling, R. F., & Rogelj, J. (2020). Changes to Carbon Isotopes in Atmospheric CO2 Over
727 the Industrial Era and Into the Future. *Global Biogeochemical Cycles*, *34*(11), 1–21.
728 https://doi.org/10.1029/2019GB006170

729 Gurney, K. R., Liang, J., Patarasuk, R., Song, Y., Huang, J., & Roest, G. (2020). The Vulcan version 3.0
730 high-resolution fossil fuel CO2 emissions for the United States. *Journal of Geophysical*
731 *Research: Atmospheres*, *125*(19), e2020JD032974.
732 Gurney, K. R., Patarasuk, R., Liang, J., Song, Y., O'Keeffe, D., Rao, P., Whetstone, J. R., Duren, R. M.,
733 Eldering, A., & Miller, C. (2019). The Hestia Fossil Fuel CO2 Emissions Data Product for the
734 Los Angeles Megacity (Hestia-LA). *Earth System Science Data Discussions*, 1–38.
735 https://doi.org/10.5194/essd-2018-162
736 Harkins, C., McDonald, B. C., Henze, D. K., & Wiedinmyer, C. (2021). A fuel-based method for
737 updating mobile source emissions during the COVID-19 pandemic. *Environmental Research*
738 *Letters*, *16*(6). https://doi.org/10.1088/1748-9326/ac0660
739 Hopkins, F. M., Kort, E. A., Bush, S. E., Ehleringer, J. R., Lai, C.-T., Blake, D. R., & Randerson, J. T.
740 (2016). Spatial patterns and source attribution of urban methane in the Los Angeles basin.
741 *Journal of Geophysical Research: Atmospheres*, *121*(5), 2490–2507.
742 https://doi.org/10.1002/2015JD024429.Received
743 Hsueh, D. Y., Krakauer, N. Y., Randerson, J. T., Xu, X., Trumbore, S. E., & Southon, J. R. (2007).
744 Regional patterns of radiocarbon and fossil fuel-derived CO2 in surface air across North America.
745 *Geophysical Research Letters*, *34*(2), L02816.
746 IPCC, 2022: Summary for Policymakers. In: Climate Change 2022: Mitigation of Climate Change.
747 Contribution of Working Group III to the Sixth Assessment Report of the Intergovernmental
748 Panel on Climate Change [P.R. Shukla, J. Skea, R. Slade, A. Al Khourdajie, R. van Diemen, D.
749 McCollum, M. Pathak, S. Some, P. Vyas, R. Fradera, M. Belkacemi, A. Hasija, G. Lisboa, S.
750 Luz, J. Malley, (eds.)]. Cambridge University Press, Cambridge, UK and New York, NY, USA.
751 doi: 10.1017/9781009157926.001.
752 Kiel, M., Eldering, A., Roten, D. D., Lin, J. C., Feng, S., Lei, R., Lauvaux, T., Oda, T., Roehl, C. M.,
753 Blavier, J. F., & Iraci, L. T. (2021). Urban-focused satellite CO2 observations from the Orbiting
754 Carbon Observatory-3: A first look at the Los Angeles megacity. *Remote Sensing of*
755 *Environment*, *258*(January). https://doi.org/10.1016/j.rse.2021.112314
756 Kort, E. A., Angevine, W. M., Duren, R., & Miller, C. E. (2013). Surface observations for monitoring
757 urban fossil fuel CO2 emissions: Minimum site location requirements for the Los Angeles
758 megacity. *Journal of Geophysical Research: Atmospheres*, *118*(3), 1577-1584.
759 Laughner, J. L., Neu, J. L., Schimel, D., Wennberg, P. O., Barsanti, K., Bowman, K. W., Chatterjee, A.,
760 Croes, B. E., Fitzmaurice, H. L., Henze, D. K., Kim, J., Kort, E. A., Liu, Z., Miyazaki, K., Turner,
761 A. J., Anenberg, S., Avise, J., Cao, H., Crisp, D., … Zeng, Z. (2021). Societal shifts due to
762 COVID-19 reveal large-scale complexities and feedbacks between atmospheric chemistry and
763 climate change. *Proceedings of the National Academy of Sciences*, *118*(46).
764 https://doi.org/10.1073/pnas.2109481118/-/DCSupplemental.Published
765 Le Quéré, C., Jackson, R. B., Jones, M. W., Smith, A. J. P., Abernethy, S., Andrew, R. M., De-Gol, A. J.,
766 Willis, D. R., Shan, Y., Canadell, J. G., Friedlingstein, P., Creutzig, F., & Peters, G. P. (2020).
767 Temporary reduction in daily global CO2 emissions during the COVID-19 forced confinement.
768 *Nature Climate Change*, 1–7. https://doi.org/10.1038/s41558-020-0797-x
769 Le Quéré, C., Peters, G. P., Friedlingstein, P., Andrew, R. M., Canadell, J. G., Davis, S. J., Jackson, R. B.,
770 & Jones, M. W. (2021). Fossil CO2 emissions in the post-COVID-19 era. *Nature Climate*
771 *Change*, *11*(3), 197–199. https://doi.org/10.1038/s41558-021-01001-0

Levin, I., Kromer, B., Schmidt, M., & Sartorius, H. (2003). A novel approach for independent budgeting of fossil fuel CO2 over Europe by 14CO2 observations. *Geophysical Research Letters*, *30*(23).

Lichtfouse, E., Lichtfouse, M., Kashgarian, M., & Bol, R. (2005). 14C of grasses as an indicator of fossil fuel CO2 pollution. Environmental Chemistry Letters, 3(2), 78-81.

Liu, D., Sun, W., Zeng, N., Han, P., Yao, B., Liu, Z., Wang, P., Zheng, K., Mei, H., & Cai, Q. (2021). Observed decreases in on-road CO2 concentrations in Beijing during COVID-19 restrictions. *Atmospheric Chemistry and Physics*, *21*(6), 4599–4614. https://doi.org/10.5194/acp-21-4599-2021

Liu, Z., Ciais, P., Deng, Z., Lei, R., Davis, S. J., Feng, S., Zheng, B., Cui, D., Dou, X., Zhu, B., Guo, R., Ke, P., Sun, T., Lu, C., He, P., Wang, Y., Yue, X., Wang, Y., Lei, Y., … Schellnhuber, H. J. (2020). Near-real-time monitoring of global CO2 emissions reveals the effects of the COVID-19 pandemic. *Nature Communications*, *11*(1), 1–12. https://doi.org/10.1038/s41467-020-18922-7

Maness, H. L., Thurlow, M. E., McDonald, B. C., & Harley, R. A. (2015). Estimates of CO2 traffic emissions frommobile concentration measurements. *Journal of Geophysical Research*, *120*(5), 2087–2102. https://doi.org/10.1002/2014JD022876

Miller, J. B., Lehman, S. J., Verhulst, K. R., Miller, C. E., Duren, R. M., Yadav, V., Newman, S., & Sloop, C. D. (2020). Large and seasonally varying biospheric CO2 fluxes in the Los Angeles megacity revealed by atmospheric radiocarbon. *Proceedings of the National Academy of Sciences of the United States of America*, *117*(43), 26681–26687. https://doi.org/10.1073/pnas.2005253117

Mitchell, L. E., Lin, J. C., Bowling, D. R., Pataki, D. E., Strong, C., Schauer, A. J., ... & Ehleringer, J. R. (2018). Long-term urban carbon dioxide observations reveal spatial and temporal dynamics related to urban characteristics and growth. *Proceedings of the National Academy of Sciences*, *115*(12), 2912-2917.

Newman, S., Xu, X., Affek, H. P., Stolper, E., & Epstein, S. (2008). Changes in mixing ratio and isotopic composition of CO2 in urban air from the Los Angeles basin, California, between 1972 and 2003. Journal of Geophysical Research: Atmospheres, 113(D23).

Newman, S., Xu, X., Gurney, K. R., Hsu, Y. K., Li, K. F., Jiang, X., Keeling, R. F., Feng, S., O'Keefe, D., & Patarasuk, R. (2016). Toward consistency between trends in bottom-up CO2 emissions and top-down atmospheric measurements in the Los Angeles megacity. *Atmospheric Chemistry and Physics*, *16*(6), 3843–3863.

Nicolini, G., Antoniella, G., Carotenuto, F., Christen, A., Ciais, P., Feigenwinter, C., Gioli, B., Stagakis, S., Velasco, E., Vogt, R., Ward., H. C., Barlow, J., Chrysoulakis, N., Duce, P., Graus, M., Helfter, C., Heusinkveld, B., Jarvi, L., Karl, T., Marras, S., Masson, V., Matthews, B., Meier, F., Nemitz, E., Sabbatini, S., Scherer, D., Schume, H., Sirca, C., Steeneveld, G., Vagnoli, C., Wang, Y., Zaldei, A., Zheng, B., & Papale, D. (2022). Direct observations of CO2 emission reductions due to COVID-19 lockdown across European urban districts. *Science of the Total Environment*, *830*, 154662.

Oda, T., Haga, C., Hosomi, K., Matsui, T., & Bun, R. (2021). Errors and uncertainties associated with the use of unconventional activity data for estimating CO2 emissions: The case for traffic emissions in Japan. *Environmental Research Letters*, *16*(8). https://doi.org/10.1088/1748-9326/ac109d

Pickers, P. A., Manning, A. C., Le Quéré, C., Forster, G. L., Luijkx, I. T., Gerbig, C., ... & Sturges, W. T. (2022). Novel quantification of regional fossil fuel CO2 reductions during COVID-19 lockdowns using atmospheric oxygen measurements. *Science advances*, *8*(16), eabl9250.

Rao, P., R. Gurney, K., Patarasuk, R., Song, Y., E. Miller, C., M. Duren, R., & Eldering, A. (2017). Spatio-temporal Variations in on-road CO2 Emissions in the Los Angeles Megacity. *AIMS Geosciences*, *3*(2), 239–267. https://doi.org/10.3934/geosci.2017.2.239

Riley, W. J., Hsueh, D. Y., Randerson, J. T., Fischer, M. L., Hatch, J. G., Pataki, D. E., Wang, W., & Goulden, M. L. (2008). Where do fossil fuel carbon dioxide emissions from California go? An analysis based on radiocarbon observations and an atmospheric transport model. *Journal of Geophysical Research: Biogeosciences*, *113*(G4).

Rosenzweig, C., Solecki, W., Hammer, S. A., & Mehrotra, S. (2010). Cities lead the way in climate-change action. *Nature*, *467*(7318), 909–911. https://doi.org/10.1038/467909a

Santos, G. M., Oliveira, F. M., Park, J., Sena, A. C. T., Chiquetto, J. B., Macario, K. D., & Grainger, C. S. G. (2019). Assessment of the regional fossil fuel CO2 distribution through Δ14C patterns in ipê leaves: The case of Rio de Janeiro state, Brazil. *City and Environment Interactions*, *1*, 100001. https://doi.org/10.1016/j.cacint.2019.06.001

Schwandner, F. M., Gunson, M. R., Miller, C. E., Carn, S. A., Eldering, A., Krings, T., Verhulst, K. R., Schimel, D. S., Nguyen, H. M., Crisp, D., O'Dell, C. W., Osterman, G. B., Iraci, L. T., & Podolske, J. R. (2017). Spaceborne detection of localized carbon dioxide sources. *Science*, *358*(6360). https://doi.org/10.1126/science.aam5782

Seto, K. C., Dhakal, S., Bigio, A., Blanco, H., Delgado, G. C., De- war, D., Huang, L., Inaba, A., Kansal, A., Lwasa, S., McMahon, J., Muller, D. B., Murakami, J., Nagendra, H., & Ramaswami, A. (2014). Human Settlements, Infrastructure, and Spatial Planning. *Climate Change 2014 Mitigation of Climate Change. Contribution of Working Group III Too the Fifth Assessment Report of the Intergovernmental Panel on Climate Change*, 923–1000. https://doi.org/10.1017/cbo9781107415416.018

Sharma, R., Kunchala, R. K., Ojha, S., Kumar, P., Gargari, S., & Chopra, S. (2023). Spatial distribution of fossil fuel derived CO2 over India using radiocarbon measurements in crop plants. *Journal of Environmental Sciences*, *124*, 19-30.

Thiruvenkatachari, R. R., Carranza, V., Ahangar, F., Marklein, A., Hopkins, F., & Venkatram, A. (2020). Uncertainty in using dispersion models to estimate methane emissions from manure lagoons in dairies. *Agricultural and Forest Meteorology*, *290*. https://doi.org/10.1016/j.agrformet.2020.108011

Trumbore, S. E., Sierra, C. A., & Hicks Pries, C. E. (2016). Radiocarbon nomenclature, theory, models, and interpretation: Measuring age, determining cycling rates, and tracing source pools. *Radiocarbon and climate change*, 45-82.

Turnbull, J. C., Miller, J. B., Lehman, S. J., Tans, P. P., Sparks, R. J., & Southon, J. (2006). Comparison of 14CO2, CO, and SF6 as tracers for recently added fossil fuel CO2 in the atmosphere and implications for biological CO2 exchange. *Geophysical research letters*, *33*(1).

Turnbull, J. C., Karion, A., Fischer, M. L., Faloona, I., Guilderson, T., Lehman, S. J., Miller, B. R., Miller, J. B., Montzka, S., Sherwood, T., Saripalli, S., Sweeney, C., & Tans, P. P. (2011). Assessment of fossil fuel carbon dioxide and other anthropogenic trace gas emissions from airborne measurements over Sacramento, California in spring 2009. *Atmospheric Chemistry and Physics*, *11*(2), 705–721. https://doi.org/10.5194/acp-11-705-2011

Turnbull, J. C., Karion, A., Davis, K. J., Lauvaux, T., Miles, N. L., Richardson, S. J., ... & Whetstone, J. (2018). Synthesis of urban CO2 emission estimates from multiple methods from the Indianapolis Flux Project (INFLUX). *Environmental science & technology*, *53*(1), 287-295.

Turnbull, J. C., Domingues, L. G., & Turton, N. (2022). Dramatic Lockdown Fossil Fuel CO2 Decrease Detected by Citizen Science-Supported Atmospheric Radiocarbon Observations. *Environmental Science & Technology*.

Turner, A. J., Kim, J., Fitzmaurice, H., Newman, C., Worthington, K., Chan, K., Wooldridge, P. J., Köehler, P., Frankenberg, C., & Cohen, R. C. (2020). Observed Impacts of COVID-19 on Urban CO2 Emissions. *Geophysical Research Letters*, *47*(22), 1–6. https://doi.org/10.1029/2020GL090037

Turner, A. J., Köhler, P., Magney, T. S., Frankenberg, C., Fung, I., & Cohen, R. C. (2020). A double peak in the seasonality of California's photosynthesis as observed from space. *Biogeosciences*, *17*(2), 405–422. https://doi.org/10.5194/bg-17-405-2020

Vargas, R., Trumbore, S. E., & Allen, M. F. (2009). Evidence of old carbon used to grow new fine roots in a tropical forest. *New Phytologist*, 710-718.

Verhulst, K. R., Karion, A., Kim, J., Salameh, P. K., Keeling, R. F., Newman, S., Miller, J., Sloop, C., Pongetti, T., Rao, P., Wong, C., Hopkins, F. M., Yadav, V., Weiss, R. F., Duren, R. M., & Miller, C. E. (2017). Carbon dioxide and methane measurements from the Los Angeles Megacity Carbon Project – Part 1: calibration, urban enhancements, and uncertainty estimates. *Atmospheric Chemistry and Physics*, *17*(13), 8313–8341. https://doi.org/10.5194/acp-17-8313-2017

Wang, W., & Pataki, D. E. (2010). Spatial patterns of plant isotope tracers in the Los Angeles urban region. *Landscape Ecology*, *25*(1), 35–52. https://doi.org/10.1007/s10980-009-9401-5

Ware, J., Kort, E. A., DeCola, P., & Duren, R. (2016). Aerosol lidar observations of atmospheric mixing in Los Angeles: Climatology and implications for greenhouse gas observations. *Journal of Geophysical Research*, *121*(16), 9862–9878. https://doi.org/10.1002/2016JD024953

Xi, X., Ding, X., Fu, D., Zhou, L., & Liu, K. (2011). Regional Δ14C patterns and fossil fuel derived CO2 distribution in the Beijing area using annual plants. *Chinese Science Bulletin*, *56*(16), 1721-1726.

Xu, X., Trumbore, S. E., Zheng, S., Southon, J. R., McDuffee, K. E., Luttgen, M., & Liu, J. C. (2007). Modifying a sealed tube zinc reduction method for preparation of AMS graphite targets: reducing background and attaining high precision. *Nuclear Instruments and Methods in Physics Research Section B: Beam Interactions with Materials and Atoms*, *259*(1), 320-329.

Yañez, C. C., Hopkins, F. M., Xu, X., Tavares, J. F., Welch, A. M., & Czimczik, C. I. (2022), Reductions in California's urban fossil fuel CO2 emissions during the COVID-19 pandemic [Dataset]. Dryad. https://doi.org/10.7280/D1F98G

Yadav, V., Ghosh, S., Mueller, K., Karion, A., Roest, G., Gourdji, S., Lopez-Coto, I., Gurney, K., Parazoo, N., Verhuslt, K. R., Kim, J., Prinzivalli, S., Fain, C., Nehrkorn, T., Mountain, M. E., Keeling, R. F., Weiss, R. F., Duren, R., Miller, C. E., & Whetstone, J. (2021). The Impact of COVID-19 on CO2 Emissions in the Los Angeles and Washington DC/Baltimore Metropolitan Areas. *Geophysical Research Letters*, *48*(11). https://doi.org/https://doi.org/10.1029/2021GL092744

Zheng, B., Geng, G., Ciais, P., Davis, S. J., Martin, R. v., Meng, J., Wu, N., Chevallier, F., Broquet, G., Boersma, F., van Der, R. A., Lin, J., Guan, D., Lei, Y., He, K., & Zhang, Q. (2020). Satellite-based estimates of decline and rebound in China's CO2 emissions during COVID-19 pandemic. *Science Advances*, *6*(49). https://doi.org/10.1126/sciadv.abd4998

Zhou, Y., Smith, S. J., Zhao, K., Imhoff, M., Thomson, A., Bond-Lamberty, B., Asrar, G. R., Zhang, X., He, C., & Elvidge, C. D. (2015). A global map of urban extent from nightlights. *Environmental Research Letters*, *10*(5), 2000–2010. https://doi.org/10.1088/1748-9326/10/5/054011